Comparative Study on MoO_3 and H_xMoO_3 Nanobelts: Structure and Electric Transport

Xiao Kai Hu,*[,†,‡] Yi Tai Qian,[‡] Z. T. Song,[†] Jia Rui Huang,[‡] R. Cao,[§] and John Q. Xiao[§]

Nanotechnology Laboratory, Research Center of Semiconductor Functional Film Engineering Technology, Shanghai Institute of Micro-system and Information Technology, Chinese Academy of Sciences, Shanghai 200050, China, Department of Chemistry, University of Science and Technology of China, Hefei, Anhui 230026, P. R. China, and Department of Physics and Astronomy, University of Delaware, Newark, Delaware 19716

Received October 11, 2007. Revised Manuscript Received November 29, 2007

In this study, the suspension of MoO_3 nanobelts was first prepared in a hydrothermal way from Mo powders and H_2O_2 solution, which could be transformed into the suspension of H_xMoO_3 nanobelts under an acidic condition using $N_2H_4 \cdot H_2O$ as the reducing agent. Three paper-form samples made from MoO_3 and H_xMoO_3 nanobelts (low or high hydrogen content) were then fabricated via a vacuum filtration method, followed by their structural comparative analysis such as FESEM, XRD, Raman spectra, and XPS, etc. The measurement of electric resistances at room temperature shows that the conductance of H_xMoO_3 nanobelts is greatly improved because of hydrogen doping. The temperature-dependent resistances of H_xMoO_3 nanobelts agree with the exponential correlation, supporting that the conducting carriers are the quasi-free electrons released from Mo^{5+}. In addition, the formation process of H_xMoO_3 nanobelts from MoO_3 nanobelts is also discussed.

Introduction

One-dimensional nanomaterials are expected to play an important role in the emerging nanoelectronics, either as functional components or conductive connections.[1,2] To this end, abundant one-dimensional functional nanostructures, including nanowires, nanotubes, and nanobelts, have been synthesized and studied extensively as the potential candidates.[3,4] Among them, carbon nanotubes have been thought to be one of the most promising alternative because of their tunable metallic or semiconducting property by chirality.[5] Doping is the fundamental and significant tool in microelectronics by which the transport property of semiconductors can be tuned continuously and various electronic devices are designed and constructed. Similarly, with respect to one-dimensional nanomaterials, the introduction of impurity atoms ought to be a critical step toward their application in future nanotechnology.

Orthorhombic molybdenum trioxide has a unique layered structure along the *b* axis, where MoO_6 octahedral double slabs are edge-connected along <001> and corner-linked along the <100> direction (see the Supporting Information, Figure S1).[6,7] The layered structure allows alkali metal cations intercalated into the van der Waals gap, accompanied by the partial reduction of Mo oxidation states.[8–11] The alkali metal molybdenum bronzes as-formed are low-dimensional metals because of the partially filled Mo 4d electrons as well as the anisotropic structure, different from the insulating MoO_3 host matrix.[12–14] The hydrogen molybdenum bronze is of particular interest in the electron/proton mixed conductance, and has been investigated for possible applications in hydrogen-transfer catalysts, electrochromic displays, fuel cells, hydrogen storage, and gas sensors.[15] The hydrogen molybdenum bronze (H_xMoO_3, $0 < x \leq 2$) phases are obtained through the reduction intercalation of MoO_3 using Zn/HCl aqueous solution or spillover approach from Pt-coated MoO_3 in hydrogen gas.[15–18] Four phases are present approximately for H_xMoO_3: nonstoichiometric phase I ($H_{0.23–0.40}MoO_3$, blue, orthorhombic), phase II ($H_{0.85–1.04}MoO_3$, blue, monoclinic), phase III ($H_{1.55–1.72}MoO_3$, red, monoclinic),

* Corresponding author. E-mail: hxk@mail.sim.ac.cn. Tel: 86-21-62511070-8405. Fax: 86-21-62134404.
† Shanghai Institute of Microsystem and Information Technology.
‡ University of Science and Technology of China.
§ University of Delaware.

(1) Javey, A.; Nam, S. W.; Friedman, R. S.; Yan, H.; Lieber, C. M. *Nano Lett.* **2007**, *7*, 773.
(2) Pauzauskie, P. J.; Sirbuly, D. J.; Yang, P. *Phys. Rev. Lett.* **2006**, *96*, 143903.
(3) Pan, Z. W.; Dai, Z. R.; Wang, Z. L. *Science* **2001**, *291*, 1947.
(4) Tsai, J. S.; Chen, F. R.; Kai, J. J. *J. Appl. Phys.* **2004**, *95*, 2015.
(5) Hu, J; Odom, T. W.; Lieber, C. M. *Acc. Chem. Res.* **1999**, *32*, 435.
(6) Lou, X. W.; Zeng, H. C. *Chem. Mater.* **2002**, *14*, 4781.
(7) Rousseau, R.; Canadell, E.; Alemany, P.; Galvan, D. H.; Hoffmann, R. *Inorg. Chem.* **1997**, *36*, 4627.
(8) Yang, Y. A.; Cao, Y. W.; Loo, B. H.; Yao, J. N. *J. Phys. Chem. B* **1998**, *102*, 9392.
(9) Bhosle, V.; Tiwari, A.; Narayan, J. *J. Appl. Phys.* **2005**, *97*, 083539.
(10) Li, C.; Xiong, R.; Yin, D.; Tang, Z.; Shi, J. *J. Cryst. Growth* **2005**, *285*, 81.
(11) Zhou, C. X.; Wang, Y. X.; Yang, L. Q.; Lin, J. H. *Inorg. Chem.* **2001**, *40*, 1521.
(12) Greenblatt, M. *Chem. Rev.* **1988**, *88*, 31.
(13) Canadell, E.; Whangbo, M. H. *Chem. Rev.* **1991**, *91*, 965.
(14) Dumas, J.; Schlenker, C.; Marcus, J.; Buder, R. *Phys. Rev. Lett.* **1983**, *50*, 757.
(15) Braida, B.; Adams, S.; Canadell, E. *Chem. Mater.* **2005**, *17*, 5957.
(16) Noh, H.; Wang, D.; Luo, S.; Flanagan, T. B. *J. Phys. Chem. B* **2004**, *108*, 310.
(17) Matsuda, T.; Uchijima, F.; Sakagami, H.; Takahashi, N. *Phys. Chem. Chem. Phys.* **2001**, *3*, 4430.
(18) Pichat, P.; Mozzanega, M. N.; Hoang-Van, C. *J. Phys. Chem.* **1988**, *92*, 467.

10.1021/cm702942y CCC: $40.75
Published on Web 01/25/2008

and stoichiometric phase IV (H_2MoO_3, green).[12,19] The properties of H_xMoO_3 vary greatly with the hydrogen content, whereas their crystal structures are all very close to that of parent MoO_3. The electric conductivity measurements on H_xMoO_3 powder or single crystal demonstrate the metal−semiconductor transition that occurs at specific temperature.[20,21,10] Most previous efforts were devoted to the understanding of the metal to semiconductor transition process induced by charge density wave or Fermi surface nesting;[12,13,20,21] fewer investigations have been performed on the semiconducting state of hydrogen molybdenum bronzes; for instance, where do conducting carriers come from?

Recently, the nanobelts of MoO_3 have been synthesized by us and other groups via the physical or chemical routes.[22–25] However, the hydrogen doping MoO_3 nanobelts were neglected in the previous study, although they are probably more important than MoO_3 nanobelts regarding the electric properties and applications in catalysis areas.[20,21,26] In this study, we synthesize the H_xMoO_3 nanobelts from MoO_3 nanobelts using a new chemical intercalation method. Structural characterization and electric transport measurement are then carried out for the two kinds of nanobelts, focusing on the relationship between structure and property.

Experimental Section

All reagents used in this work were chemical-grade reagents from the Shanghai Chemical Factory, P. R. China, and were directly used without further treatment.

Synthesis of MoO_3 Nanobelts. The synthetic strategy is the same as that described previously by us.[22] In a typical procedure, molybdenum powders (2 mmol), deionized water (40 mL), and 30 wt% H_2O_2 aqueous solution (2∼4 mL) were successively added into a Teflon vessel (60 mL). The vessel was then heated at 70 °C under magnetic agitation until metal powders were dissolved completely. Subsequently, the vessel was transferred into a stainless steel autoclave and hydrothermally treated at 140 °C for 12 h. After natural cooling, the white aqueous suspensions of MoO_3 nanobelts were obtained and used directly for preparation of H_xMoO_3 nanobelts in the next step. In addition, the paper, which was composed of MoO_3 nanobelts, was fabricated from the suspensions through the vacuum filtration method, followed by the drying and peeling processes, labeled sample A. No binding agent is used in the fabrication process.

Synthesis of H_xMoO_3 Nanobelts. First, 4 mL of 2.3 M HCl solution was added to the suspension of MoO_3 nanobelts (∼40 mL), to ensure a strong acidic environment and enough proton sources. Second, under vigorous magnetic stirring, the hydrated hydrazine solution (85 wt% $N_2H_4\cdot H_2O$) was introduced dropwise to the suspension, leaving enough time for reaction after each drop's addition (ca. 50 μL for one drop). In this way, the suspension gradually changed in color from initial white to intermediate blue and to dark blue in the end, indicating the conversion from MoO_3 nanobelts to H_xMoO_3 nanobelts because of hydrogen increasing insertion. Similarly, the papers of H_xMoO_3 nanobelts, labeled sample B (blue) and sample C (dark blue), were also fabricated through the vacuum filtration method followed by the drying and peeling processes, both of which were obtainable with one and six drops of $N_2H_4\cdot H_2O$ solution titrated, respectively. For the purpose of comparison, the H_xMoO_3 nanobelts were also prepared using the conventional Zn/HCl reduction/intercalation method.

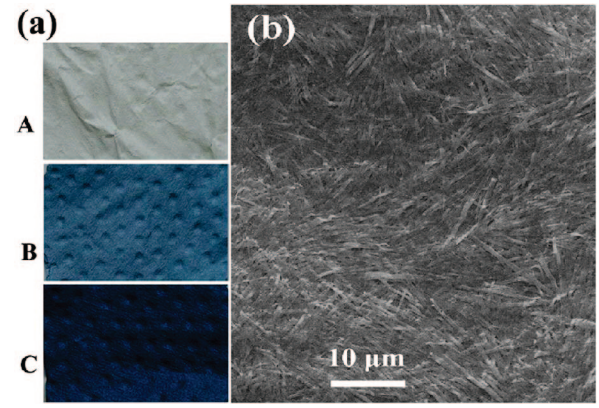

Figure 1. (a) Photos of samples A, B, and C, which are made from MoO_3 nanobelts and H_xMoO_3 nanobelts with low and high hydrogen content, respectively. (b) Typical magnified FESEM image of H_xMoO_3 nanobelts (sample C).

Characterization. The nanobelts were characterized by X-ray diffraction (XRD, Phillip X'pert system, $\lambda = 1.541874$ Å), Raman spectrum (RAMANLOG-6 laser Raman spectrometer), field-emission scanning electron microscopy (FESEM, JEOL JSM-6300F), transmission electron microscopy (TEM, Hitachi 800 operated at 200 kV) with selected area electron diffraction (SAED), X-ray photoelectron spectrum (XPS, ESCALAB 250 with monochromatized Mg Kα X-ray as the source), high-resolution transmission electron microscopy (HRTEM, JEOL 2010 working at 200 kV), and photoluminescence spectrum (PL, FLUOROLOG-3-TAU steady-state/lifetime spectrofluorometer).

Measurement of Electric Resistances. The paper-form samples were cut into 3 cm × 1 cm strips for four-probe measurements. The electrode contacts were made by using conductive silver pastes prior to desiccation in a vaccum at 100 °C. The $I-V$ curves of samples A, B, and C at room temperature (RT) were recorded on the conventional four-probe setup, within the voltage range from −1 to +1 V. Their RT resistances were calculated according to the slopes of curves, respectively. In addition, the resistances of sample C as a function of temperature were measured in the course of cooling from room temperature (290 K) to low temperature (150 K), during which a constant electric current of 0.1 mA was supplied.

Results and Discussion

Color and Morphology. Three samples are fabricated in the present study, including sample A (MoO_3 nanobelts, white), sample B and C (H_xMoO_3 nanobelts with low and high hydrogen content, blue and dark blue, respectively), as shown in Figure 1a. The paper-form samples are fabricated using a simple vacuum filtration method, as described in the experimental section, which has also been adopted to fabricate carbon nanotube films.[27] The blue color of H_xMoO_3

(19) Hirata, T.; Ishioka, K.; Kitajima, M. *Appl. Phys. Lett.* **1996**, *68*, 458.
(20) Adams, S.; Ehses, K. H.; Spilker, J. *Acta Crystallogr., Sect. B* **1993**, *49*, 958.
(21) Adams, S. *J. Solid State Chem.* **2000**, *149*, 75.
(22) Hu, X. K.; Ma, D. K.; Xu, L. Q.; Qian, Y. T. *Chem. Lett.* **2006**, *35*, 962.
(23) Li, X. L.; Liu, J. F.; Li, Y. D. *Appl. Phys. Lett.* **2002**, *81*, 4832.
(24) Li, Y. B.; Bando, Y.; Golberg, D.; Kurashima, K. *Appl. Phys. Lett.* **2002**, *81*, 5048.
(25) Xia, T.; Li, Q.; Liu, X.; Meng, J.; Cao, X. *J. Phys. Chem. B* **2006**, *110*, 2006.
(26) Li, W.; Lu, J.; Du, J.; Lu, D.; Wu, Y. *Electrochem. Commun.* **2005**, *7*, 406.

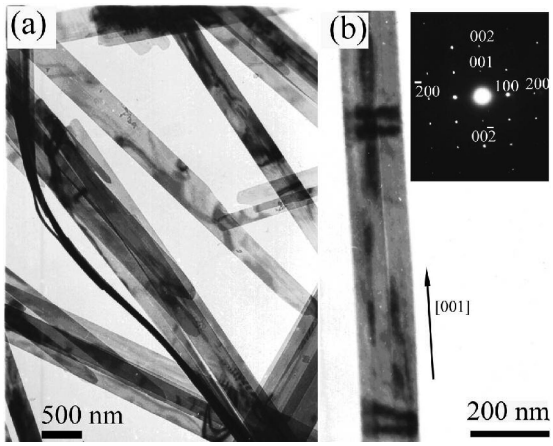

Figure 2. (a) TEM image of MoO_3 nanobelts. (b) TEM image of an individual MoO_3 nanobelt and its SAED pattern.

nanobelts originates from the inter valence charge-transfer transition between Mo^{5+} and Mo^{6+} that coexist in H_xMoO_3 nanobelts.[8] Figure 1b is a representative FESEM image of H_xMoO_3 nanobelts (sample C), from which it can be seen that the nanobelts, approximately ten micrometers in length, have a preferential stacking orientation with their wide facets spreading on the paper but a random longitudinal array. Although the papers are not highly dense in view, the nanobelts within are contacted well with one another. Additionally, there is no difference in morphology and topology between MoO_3 nanobelts and H_xMoO_3 nanobelts, by comparing their FESEM images. Figure 2a is the TEM image of pristine MoO_3 nanobelts, showing that the nanobelts have a typical width of 100−500 nm, and a thickness of about 20−30 nm, as estimated from the bended parts. Figure 2b is a single MoO_3 nanobelt and its SAED pattern (corresponding to [010] zone axis), illustrating that nanobelts grow in the [001] direction and their wide facet corresponds to (010) crystalline plane of MoO_3.[23,24]

X-ray Diffraction Analysis. Figure 3 demonstrates the XRD patterns of the three samples that are fully ground prior to diffraction. The three patterns in Figure 3a are very analogous as a whole, and in combination with the JCPDS card (05–0508) of orthorhombic MoO_3, we conclude that the three-dimensional structural framework of MoO_3 nanobelts is retained to a great degree in H_xMoO_3 nanobelts, and hydrogen doping does not destroy the pristine crystal structure.[19] Therefore, H_xMoO_3 inherits the beltlike morphology of MoO_3. Figure 3b−d are the magnified patterns corresponding to the diffraction peaks of (040), (060), and (002) in Figure 3a, respectively. Careful comparison among these patterns discloses that the 2θ values (peak positions) decrease slightly from A to B, but do sharply from B to C. The smaller 2θ value means larger interplane distance (d value), according to Bragg Formula $2\,d\sin\theta = \lambda$. Hence, with the increasing insertion of hydrogen into H_xMoO_3 nanobelts (sample A, $x = 0$), the distances (d values) between crystalline planes of (040), (060), and (002) increase consistently. That is, the lattice unit expands after hydrogen atoms are introduced into MoO_3, as reflected on the

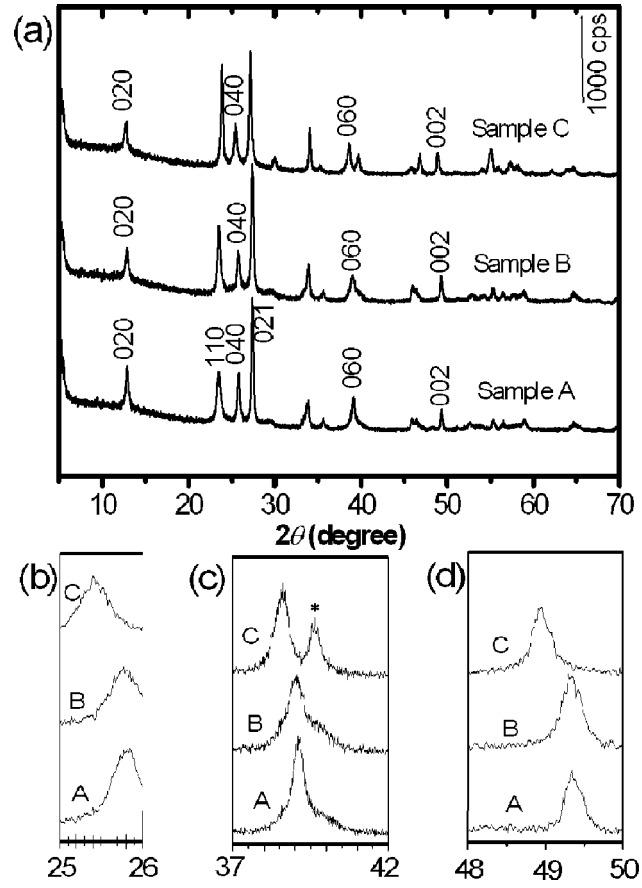

Figure 3. (a) Overall XRD patterns of samples A, B, and C, consisting of MoO_3 nanobelts and H_xMoO_3 nanobelts with low and high hydrogen content, respectively. (b−d) magnified patterns corresponding to the diffraction peaks of (040), (060), and (002) in (a), respectively.

Table 1. Lattice Constants a, b, and c Calculated by $d_{(200)}$, $d_{(060)}$, and $d_{(002)}$

sample	hydrogen content (x)	interplane distance (Å)			lattice constants (Å)		
		$d_{(060)}$	$d_{(002)}$	$d_{(200)}$	a	b	c
A	zero	2.3009	1.8479	1.9768	3.954	13.805	3.696
B	low	2.3067	1.8481	1.9763	3.953	13.840	3.696
C	high	2.3261	1.8622	1.9825	3.965	13.957	3.724

calculated lattice constants that are listed in Table 1. In Figure 3c, the peak indicated with an asterisk becomes more pronounced in C as compared in B and A, probably hinting that slight structural adjustment occurs when the hydrogen content is high.

Raman Spectra. The Raman spectra of the three samples are compared in Figure 4, with the same instrumental conditions such as laser spot area and detection time. Curve A is the Raman spectrum of MoO_3 nanobelts, in which all peaks in position are in good agreement with the polycrystalline MoO_3 powders in the literatures.[28] Specifically, the peak at 995 cm^{-1} is assigned to the terminal oxygen (Mo═O) stretching mode, the peak at 818 cm^{-1} to the doubly coordinated bridging oxygen (Mo_2−O) stretching mode, and the peak at 664 cm^{-1} to the triply coordinated oxygen

(27) Zhang, D.; Ryu, K.; Liu, X.; Polikarpov, E.; Tompson, M. E.; Zhou, C *Nano Lett.* **2006**, *6*, 1880.

(28) Mestl, G.; Ruiz, P.; Delmon, B.; Knozinger, H. *J. Phys. Chem.* **1994**, *98*, 11269.

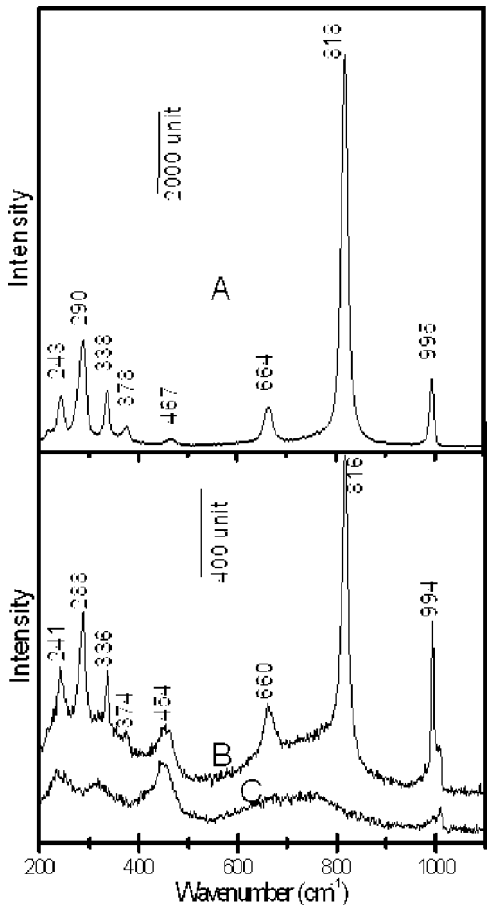

Figure 4. Room-temperature Raman spectra of samples A, B, and C measured under the same conditions.

(Mo_3−O) stretching mode.[29] The sharpness of peaks in curve A represents the high crystalline state and excellent structural order in MoO_3 nanobelts. Curve B gives the Raman spectrum of sample B, all peaks easily corresponding to those in curve A. However, some differences are present between the Raman spectrum of samples A and B. First, the intensity is obviously low in sample B. Second, all peaks in sample B shift toward low wavenumber, slightly and unanimously. Third, most peaks in sample B broaden with respect to the full width at half-maximum (fwhm). On the basis of the above XRD analysis, the crystalline lattice of sample B expands slightly relative to sample A, and small structural distortions likely happen on sample B as well, as a result of hydrogen intercalation. Therefore, the structural order is lowered in sample B, which can lead to the decreased Raman vibrational intensity and peak broadening. The peak shifts in the Raman spectrum are related to changes in the force constants of the bonds, i.e., positive and negative shifts correspond to larger and smaller force constants, respectively.[29] Because the lattice is enlarged in sample B, the force constants of bonds become small and the peaks shift to lower wavenumbers. Generally, the Raman spectra are more sensitive than XRD detection to the structure change.[30] Curve C exhibits the Raman spectrum of sample C that has high

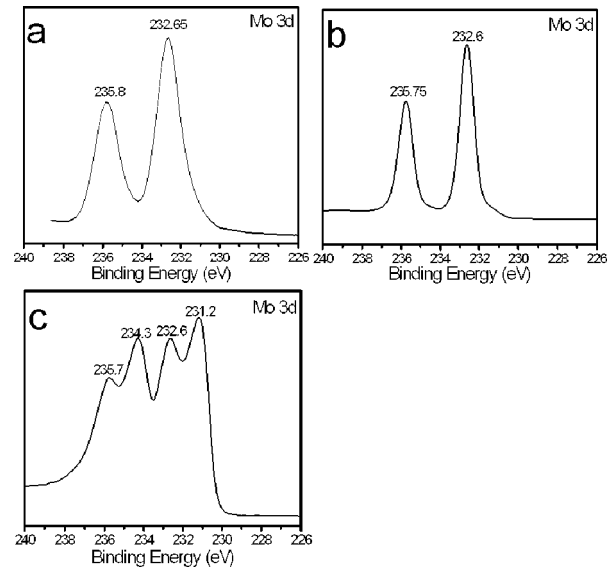

Figure 5. Room-temperature Mo3d-related XPS spectra of samples (a) A, (b) B, and (c) C.

hydrogen content. The Raman peaks decrease greatly in intensity, as compared to those of sample A and B. Because of the large lattice expansion and structural distortion, some peaks are not observed. In addition, the delocalized electrons present in samples B and C (see below) may play a role in the intensity reduction because of their screening effect on phonons.[19]

X-rays Photoelectron Spectra. The XPS spectra recorded on the three samples are demonstrated in Figure 5, with molybdenum element being concerned. The doublets of binding energy reflect the Mo oxidation states present in MoO_3 or H_xMoO_3 nanobelts. In Figure 5a, the doublets of 235.8 and 232.65 eV are attributed, respectively, to the binding energies of the $3d_{3/2}$ and $3d_{5/2}$ electrons of Mo^{6+}, which are present exclusively in MoO_3 nanobelts.[31] The integral areas between the two doublets are 2:3 in ratio and the energy gap between them is 3.15 eV, in agreement with the standard data.[32] In Figure 5b, in the case of H_xMoO_3 nanobelts with low hydrogen content, the two peaks shift to low energy slightly, as compared to those in Figure 5a. It is known that the extra electron screening can lower the inner electron binding energy of core metallic cations. Therefore, we infer that in H_xMoO_3 nanobelts, although some molybdenum has been reduced to Mo(V) in the hydrogen intercalation process, the additional electron of Mo^{5+} relative to Mo^{6+} is actually delocalized to a great degree at room temperature and not binded tightly to an individual Mo^{6+} core cation. These delocalized electrons extend mainly within the MoO_6 octahedral double slabs of MoO_3. In this regard, it is reasonable that only one set of doublets is detected, with slight decreases in the corresponding binding energies due to the screening effect of delocalized electrons (Figure 5b). However, when the doped hydrogen concentration is high in sample C, the situation is different. As shown in Figure

(29) Ajito, K.; Nagahara, L. A.; Tryk, D. A.; Hashimoto, K.; Fujishima, A *J. Phys. Chem.* **1995**, *99*, 16383.
(30) Sattar, A.; Srivastava, J. P.; Sharma, S. V.; Khulbe, P. K.; Bist, H. D. *J. Raman Spectrosc.* **1997**, *28*, 1005.
(31) Bica de Moraes, M. A.; Trasferetti, B. C.; Durrant, S. F.; Urbano, A. *Chem. Mater.* **2004**, *16*, 513.
(32) Wagner, C. D.; Riggs, W. M.; Davis, L. E.; Moulder, J. F.; Muilenberg, G. E. *Handbook of X-ray Photoelectron Spectroscopy*; Perkin-Elmer Corporation: Waltham, MA, 1978.

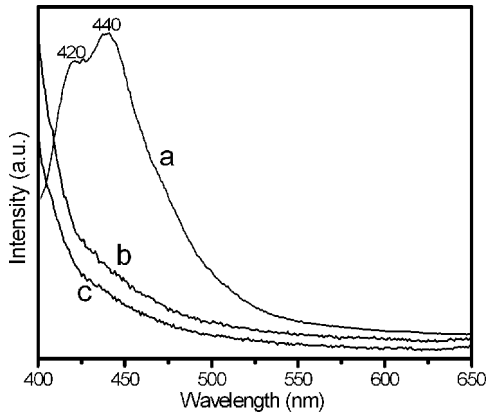

Figure 6. Photoluminescence spectra of samples (a) A, (b) B, and (c) C, under the excitation wavelength of 370 nm.

5c, two sets of doublets are detected, one being ascribed to Mo^{6+} (235.7 and 232.6 eV corresponding to $3d_{3/2}$ and $3d_{5/2}$ of Mo^{6+}) and the other to Mo^{5+} (234.3 and 231.2 eV corresponding to $3d_{3/2}$ and $3d_{5/2}$ of Mo^{5+}).[31,32] The more protons intercalated, the more electrons injected in the meantime. Thus, in addition to a fraction of electrons that are still delocalized, the other electrons have to be restricted around the Mo^{6+} core cations, and as a result, the Mo^{5+} cations are detected in the XPS spectrum of sample C.

In fact, the above discussion has assumed that the hydrogen are always present in the protonic state. Previous study on hydrogen molybdenum bronze believed that there were two different types of sites available for proton occupation, interlayer sites between the van der Waals gaps and intralayer sites within the zigzag channels along the *c* axis.[15] The investigations of ^1H NMR or neutron diffraction experiments show that the hydrogen are bonded to the terminal oxygen atoms O(3) with group OH_2 or bridging oxygen atoms O(2) with group OH.[20,21] In other word, the doped hydrogens are present in the MoO_3 lattice at interstitial sites and bond to oxygen atoms of MoO_6 octahedron.

Photoluminescence Spectra. In our previous study, the PL spectra have been employed to distinguish the MoO_3 and H_xMoO_3 nanobelts.[22] Here, the PL spectra of three samples are outlined in Figure 6. The presence of emission peaks in curve a shows the radiative recombination of interband electrons and holes in MoO_3 nanobelts. On the contrary, no emission peaks are observed in curve b or c, which means the difference in electronic structure between MoO_3 and H_xMoO_3 nanobelts. The existence of Mo^{5+} in H_xMoO_3 nanobelts may create trapping states in a forbidden band, which can trap electrons, making the interband recombination not happen again.[33]

High-Resolution Transmission Electron Microscopy Images. Figure 7a demonstrates the HRTEM image of a single MoO_3 nanobelt and its SAED pattern (inserted picture). MoO_3 nanobelt is well-resolved regarding its lattice fringes. The lattice spacing of (001) and (100) planes are about 3.7 and 3.9 Å, respectively.[22–25] The 1.8 Å spacing of (002) planes is also visible. In contrast, the lattice fringes of the heavy doped H_xMoO_3 nanobelt (sample C), as seen in its HRTEM image (Figure 7b), are not as clear as those of MoO_3 nanobelt. For example, the crystalline lattices of the H_xMoO_3 nanobelt are no longer continuous on the whole, and many parts are distorted or dislocated seriously. In addition, very often, the SAED pattern of H_xMoO_3 nanobelt differs from that of MoO_3 nanobelt, with many diffraction spots being absent, as shown in the inset of Figure 7b. The structural order in the H_xMoO_3 nanobelt is disturbed because of the hydrogen doping, consistent with the conclusions drawn from the XRD and Raman investigations.

Formation Process of Hydrogen Molybdenum Bronze. In the acidic environment, the standard electrode potential of hydrated hydrazine ($N_2H_4 \cdot H_2O$) is -0.23 V, and its oxidized product is nitrogen gas, which makes the post-treatment process convenient. The standard hydrogen potential is zero. Therefore, in our case, the protons are probably reduced by $N_2H_4 \cdot H_2O$ to active hydrogen atoms at first, and in the presence of MoO_3 nanobelts, these atomic hydrogens then directly intercalate into the MoO_3 lattice and bond to oxygen, and their electron is transferred to molybdenum cations.[18] The half-and overall reactions associated with the reduction-intercalation process are expressed as follows:

$$N_2 + 5H^+ + 4e = N_2H_5^+ \quad E^o = -0.23\ V$$

$$N_2H_5 + 4H^+ + 4/xMoO_3 = 4/xH_xMoO_3 + N_2\uparrow + 5H^+$$

In the intercalation process, the strong acidic environment is a necessity, not only in providing enough of a proton source but also in keeping MoO_3 stable; otherwise, MoO_3 easily dissolves in basic $N_2H_4 \cdot H_2O$ solution. The intercalation reaction is not fast, and the suspension of nanobelts gradually changes in color from white to blue and to dark blue with more atomic hydrogen being inserted. Therefore, the hydrogen concentration is controllable in the H_xMoO_3 nanobelt by the amount of hydrated hydrazine added.

In comparison, we also adopt the conventional Zn/HCl intercalation method to prepare hydrogen bronzes, and their FESEM image is shown in Figure 8. We find that the H_xMoO_3 nanobelts prepared in this way often coexist with the unreacted zinc particles. The replacement of liquid hydrated hydrazine by particulated zinc as reducing agent can accelerate the intercalation process on the one hand because of the stronger reducing ability of Zn ($E^o = -0.76$ V) but, on the other hand, makes the separation of unreacted metal difficult. Thus, hydrated hydrazine may be superior to zinc as a reducing agent in the fabrication of H_xMoO_3 nanobelts.

Electric Transport of the Three Nanobelts. Figure 9 shows the $I-V$ curves of the three samples measured at room temperature. The $I-V$ linearity shows the three samples follow the ohmic behavior, by which the calculated electric resistances of sample A, B, and C are 19.44 MΩ, 1.70 MΩ, and 384.5 Ω, respectively. It is obvious that with the insertion of protons, the conductance of H_xMoO_3 nanobelts is enhanced. The conductance of MoO_3 is ascribed to the electrons present in conductive band and holes in valence band. Because the band gap of MoO_3 is relatively large, the intrinsic carrier concentration is low and the resistance is huge. As to sample B with little doped hydrogen, the "free"

(33) Yao, J. N.; Yang, Y. A.; Loo, B. H. *J. Phys. Chem. B* **1998**, *102*, 1856.

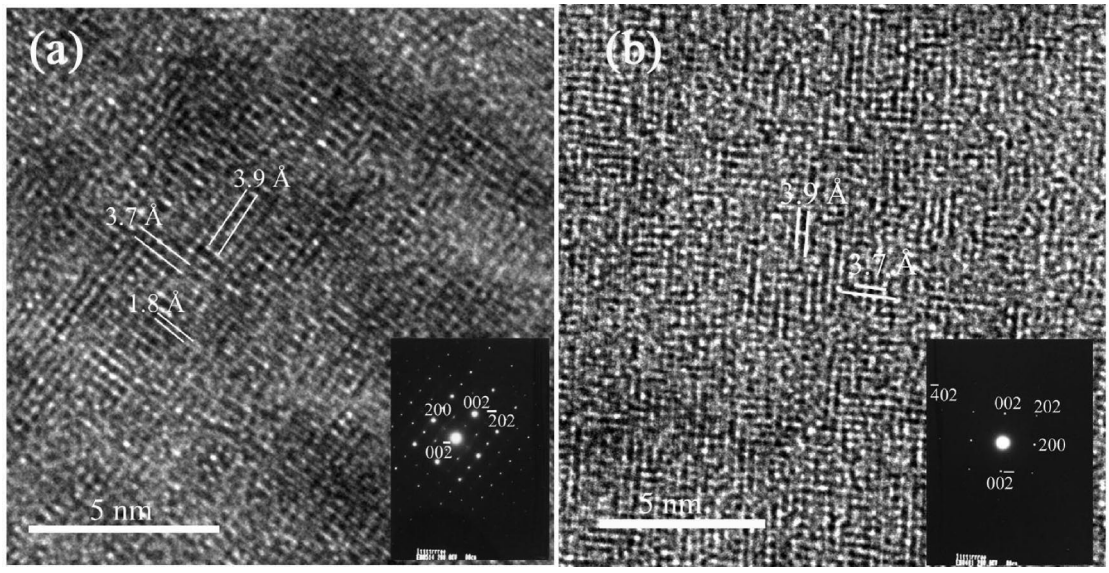

Figure 7. HRTEM images of one MoO_3 (a, sample A) and H_xMoO_3 nanobelt (b, sample C) with the corresponding SAED patterns inserted.

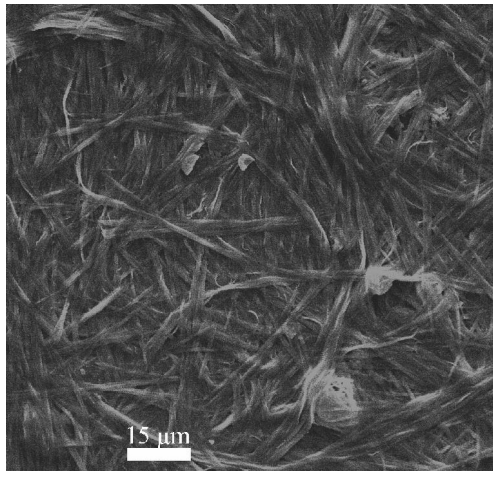

Figure 8. FESEM image of H_xMoO_3 nanobelts fabricated by the conventional Zn/HCl method instead of present $N_2H_4 \cdot H_2O$/HCl method, showing that the unreacted Zn particles are hard to be removed.

electrons are present in MoO_6 octahedral double slabs, as inferred from XPS data, and are the dominant carriers for enabling its conductance to increase more than 1 order of magnitude, in comparison with sample A. In sample C, however, the quasi-free electrons within the oxide's structural layers are much higher in concentration, accounting for its lowest resistance. The resistance of sample C is only less than 1/50 000 that of sample A.

Figure 10 demonstrates the relationships of resistance versus temperature for H_xMoO_3 nanobelts (sample C). Figure 10b and its inset are parts of Figure 10a, and Figure 10c derives from Figure 10a by plotting $\ln R \approx 1/T$. Obviously, the resistance of H_xMoO_3 nanobelts increases almost in an exponential way with temperature lowered, complying with the $R-T$ relation $R = R_0 \exp(\epsilon/k_BT)$, where R_0 can be believed a constant for a given sample with specific dimensions, and ϵ is the thermally activated energy of electron from Mo^{5+} to Mo^{6+}, k_B is the Boltzmann constant, and T is Kelvin temperature. As the temperature decreases, the quasi-free electrons present in H_xMoO_3 nanobelts are trapped by Mo^{6+}, and the number of conducting electrons is reduced

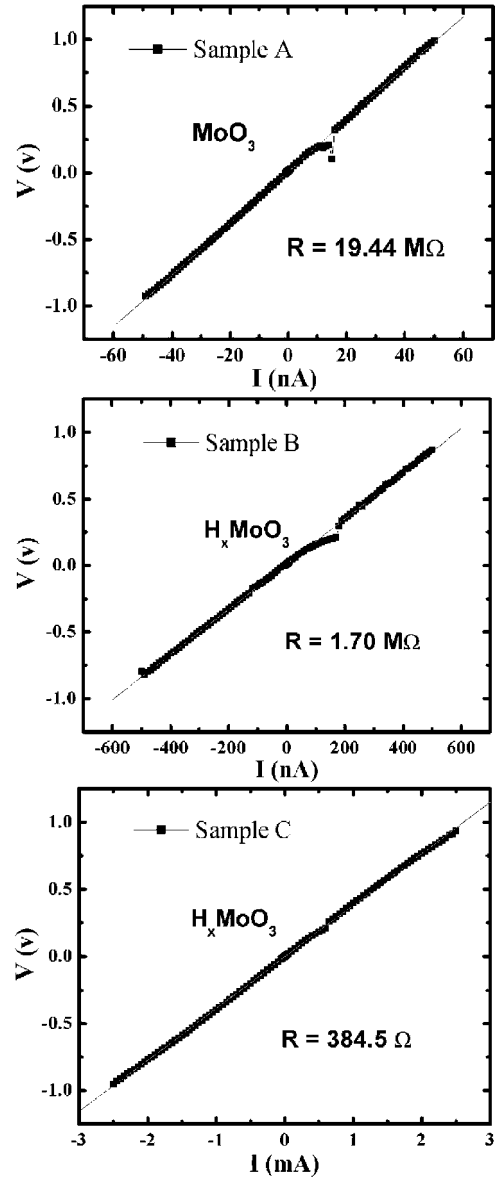

Figure 9. $I-V$ curves of samples A, B, and C at room temperature.

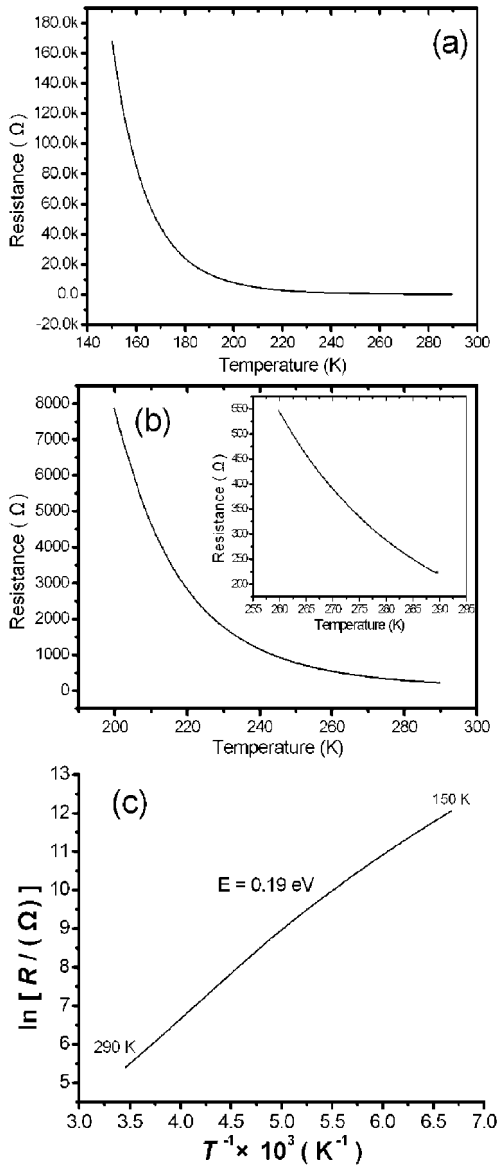

Figure 10. Correlation of electric resistance versus temperature regarding H_xMoO_3 nanobelts of sample C.

exponentially by $n = n_0\exp(-\epsilon/k_BT)$, where n_0 is related to the x value in H_xMoO_3 nanobelts. It seems that the oxide structural layers (or MoO_6 octahedral double slabs) behave as an electron reservoir or well, as contrast to the graphite sheets. In comparison with the previous results by Adams et al.,[20] where electric conductivity of H_xMoO_3 powder sample (phase I) follows the Arrhenius equation from room temperature to 390 K in addition to a metal-semiconductor transition at 400 K, the activated energy ϵ seems to have a distinct meaning in this context. The departure of ln $R \approx 1/T$ from strict linear relation may come from the variation of electron mobility at different temperature. Roughly, according to the slope of ln $R \approx 1/T$ in Figure 10c, the activated energy ϵ is determined to be 0.19 eV, which is comparable to Adams' value.[20] Thus, the activated or passivated process concerning quasi-free electrons can be described as follows: $Mo^{5+} + \epsilon \leftrightarrow Mo^{6+} + e$. By taking the sample's dimension into account, the resistivity of sample C at room temperature is about 0.45 Ω cm.

Conclusions

Uniform MoO_3 nanobelts can be fabricated hydrothermally from molybdenum and hydrogen peroxide. The controllable hydrogen doping (H_xMoO_3, hydrogen molybdenum bronze) of nanobelts can be realized by using hydrazine solution as reducing agent in acidic media. With the increasing insertion of hydrogen, the crystal lattice of oxide expands and structural order deteriorates. The transitional metallic cations are present with mixed valences in H_xMoO_3 nanobelts. The Mo^{5+} may release the extra electron to the oxide's structural layer because of thermal fluctuation. These released electrons are quasifree within the MoO_6 octahedral double slabs but restricted along the b axis of MoO_3. The electric conductance of H_xMoO_3 nanobelts is enhanced greatly thanks to hydrogen doping. The electric resistance of H_xMoO_3 nanobelts rises exponentially with the temperature being lowered. According to our calculation, the activated energy of electron from Mo^{5+} to Mo^{6+} is 0.19 eV. The fabrication of H_xMoO_3 nanobelts provides an opportunity for exploring the complex physical properties of molybdenum bronzes. In addition, H_xMoO_3 nanobelts may present another choice as building blocks for the integration of nanoscale electronic devices in future technology.

Acknowledgment. The authors greatly acknowledge the financial support from the 973 project of China (2005CB623601) and Professor K. Q. Ruan at the Department of Physics at USTC for his help.

Supporting Information Available: The crystal structure of orthorhombic α-MoO_3 (PDF). This material is available free of charge via the Internet at http://pubs.acs.org.

CM702942Y